

Comparative Analysis of Hydrogen-Bonding Vibrations of Ice VI

Xue-Chun Wang, Xu-Liang Zhu, Yue Gu, Hao-Cheng Wang, Xiao-Ling Qin, Jing-Wen Cao, Xu-Hao Yu, Xiao-Qing Yuan, and Peng Zhang*



Cite This: *ACS Omega* 2021, 6, 14442–14446



Read Online

ACCESS |



Metrics & More

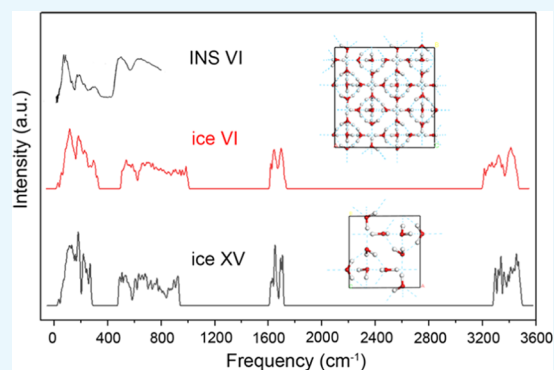


Article Recommendations



Supporting Information

ABSTRACT: It is difficult to investigate the hydrogen-bonding dynamics of hydrogen-disordered ice VI. Here, we present a comparative method based on our previous study of its counterpart hydrogen-ordered phase, ice XV. The primitive cell of ice XV is a 10 molecule unit, and the vibrational normal modes were analyzed individually. We constructed an 80 molecule supercell of ice VI to mimic the periodic unit and performed first-principles density functional theory calculations. As the two vibrational spectra show almost identical features, we compared the molecular translation vibrations. Inspired by the phonon analysis of ice XV, we found that the vibrational modes in the translation band of ice VI are classifiable into three groups. The lowest-strength vibration modes represent vibrations between two sublattices that lack hydrogen bonding. The highest-strength vibration modes represent the vibration of four hydrogen bonds of one molecule. The middle-strength vibration modes mainly represent the molecular vibrations of only two hydrogen bonds. Although there are many overlapping stronger and middle modes, there are only two main peaks in the inelastic neutron scattering (INS) spectra. This work explains the origin of the two main peaks in the far-infrared region of ice VI and illustrates how to analyze a hydrogen-disordered ice structure.



1. INTRODUCTION

Following the discovery of ice II and ice III by Tammann,¹ the phase diagram was extended by Bridgman,^{2–4} who discovered ices IV, V, VI, and VII. Since then, further 20 crystalline phases of ice have been found to exist under different temperatures and pressures,^{5–17} with ice XIX being the latest.¹⁷ Interestingly, most of these phases exist in pairs, such as ice VI and ice XV, which have the same oxygen sublattice structure but differ in terms of hydrogen order or disorder. Thus, ice VI is the hydrogen-disordered counterpart of ice XV. Recently, Gasser et al. found that below 103 K, there is a thermodynamically more stable structure ice β -XV than ice XV,¹⁸ which was recently named ice XIX.¹⁷ McFarlan reported that ice VI is indefinitely stable at 118 K at ordinary pressure.^{19,20} Bertie et al. were the first to prepare ice VI in a laboratory, which they achieved using a high-pressure apparatus.²¹ Block developed a method for studying single crystals of ice VI by X-ray diffraction under high pressure.²² Kamb determined the structure of ice VI, revealing that it was composed of two interpenetrating but non-interconnecting frameworks, such that the complete structure can be considered a “self-clathrate”.²³ This work was performed via neutron powder diffraction.²⁴ In addition to these X-ray and neutron powder diffraction experiments, INS spectra analyses have been conducted.²⁵ In addition, Fan et al. have performed calculations to develop a comprehensive understanding of the structure of ice VI.²⁶

Hydrogen-ordered ice XV was discovered by Salzmann et al. in 2009, and it is thought to be thermodynamically stable at less than -130 K and at 0.8 – 1.5 GPa.¹³ More recently, Whale et al. reported new types of vibrational normal modes for ice XV, namely, an O–H “isolated” stretching mode and “rigid network” molecular translational vibrations.²⁷ We have reviewed the vibrational normal modes of ice XV and clarified the physical aspects of its exotic vibrational modes.²⁸ The distributions of vibrational modes in ice XV are similar to those we have determined in our previous series of studies, such as ice VII and VIII, and the hydrogen-bonding modes in the translational band also obey the theory of two types of hydrogen bonds.^{29–40} Based on a successful investigation of ice XV, in this study, we constructed an ice VI supercell, explored its atomic and molecular vibrational modes, and compared these modes with those of ice XV. A comparative analysis was also reported in the meaning of an experimental method. Such as Abe et al. confirmed the existence of LO–TO splitting in ice for the first time by comparing the Raman spectra of ice XI and Ih,⁴¹ and Gasser et al. discovered a new stable phase ice β -XV through the comparative experiments between ice XV and

Received: March 11, 2021

Accepted: May 13, 2021

Published: May 25, 2021



VI.¹⁸ We focused on the hydrogen-bonding vibrations in the translation band and endeavored to determine the origin of the vibrational peaks in the far-infrared region.

2. RESULTS AND DISCUSSION

Figure 1 shows a comparison of the calculated phonon density of states (PDOS) of ice VI and ice XV, together with the INS

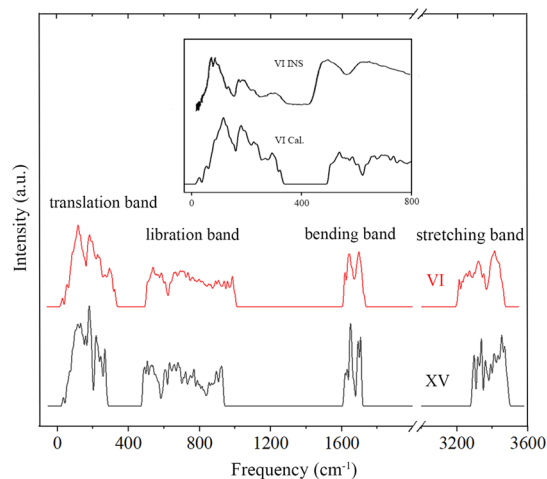


Figure 1. Comparison of simulated spectra of ice VI and ice XV. The four separate vibrational bands are (from left to right) the translation band, the libration band, the bending band, and the stretching band. The inset illustrates the good agreement between the INS data⁴² and the calculated data for ice VI.

data of the translation band.⁴² Recently, Rosu-Finsen et al. studied the deep-glassy ice VI, and the INS data of ice VI is the same as the data in the illustration.⁴³ It can be seen that there is good agreement between the calculated spectrum and the INS data in this region. The INS data was from TOSCA instrument in ISIS, Rutherford Appleton laboratory. The best resolution is below 200 meV, especially for the translation band. Since we focus on hydrogen bonding in this work, we can compare the INS directly with PDOS. According to our previous comparative investigation on ices VII and VIII,³⁶ the calculated spectrum of ice VI is smoother than that of ice XV. This is due to the primitive cell of ice XV containing only 10 molecules. Hence, in ice XV, there are 87 ($10 \times 3 \times 3 - 3$) optical branches of dispersion curves, while ice VI contains 717 ($80 \times 3 \times 3 - 3$) optical branches within an 80 molecule supercell. Due to its H-disordered structure, all of the phonon states of ice VI are nondegenerate, meaning that many states overlap, and thus ice VI has a smoother dispersion curve than ice XV. In addition, the translation band of ice VI is blue-shifted while the stretching band is red-shifted compared to those of ice XV.

As the INS experiment collected the phonon signals throughout the entire first Brillouin zone, the INS spectrum is proportional to the calculated PDOS spectrum. Thus, we were able to directly compare the PDOS curve with the INS curve. Li et al. have reported the INS spectrum of ice VI.²⁵ There are several notable peaks in this spectrum at 21.4, 23.8, 28.6, and 37.3 meV (172.3, 191.6, 230.2, and 300.2 cm^{-1}), which correspond to 179.5, 193.2, 236.6, and 294.6 cm^{-1} in the translation region in this work. The experimental peak is at

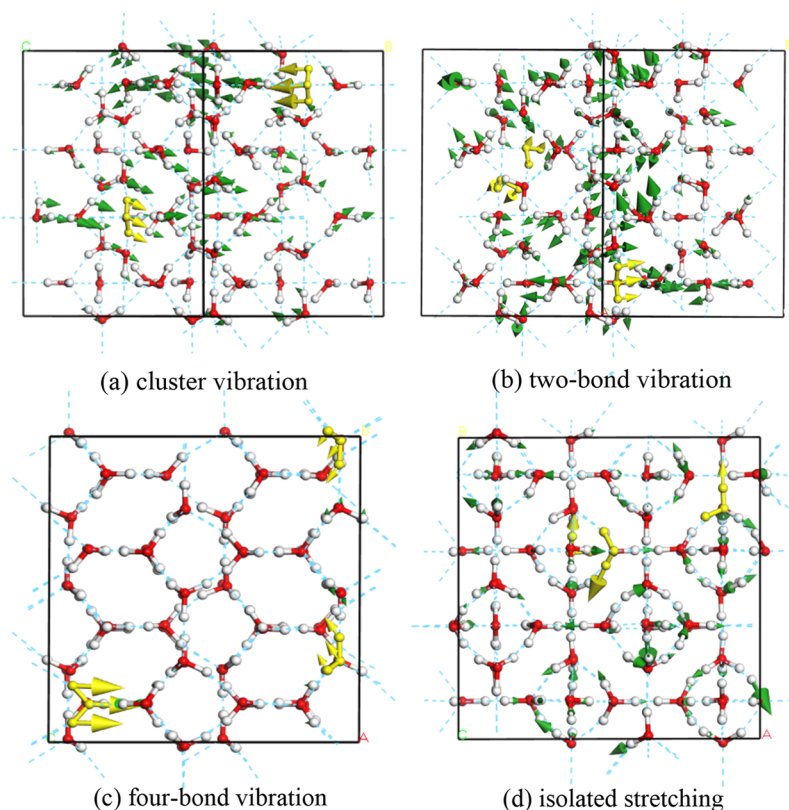


Figure 2. Examples of vibrational normal modes of ice VI in the translation band at (a) cluster vibration at 46 cm^{-1} , (b) two-bond vibration at 231 cm^{-1} , (c) four-bond vibration at 328 cm^{-1} , and (d) isolated stretching of one normal vibrational mode at 3378 cm^{-1} in the stretching band, which represents an isolated vibration. The arrows indicate the vibrational direction of the atoms, while gold arrows present typical molecular vibrations.

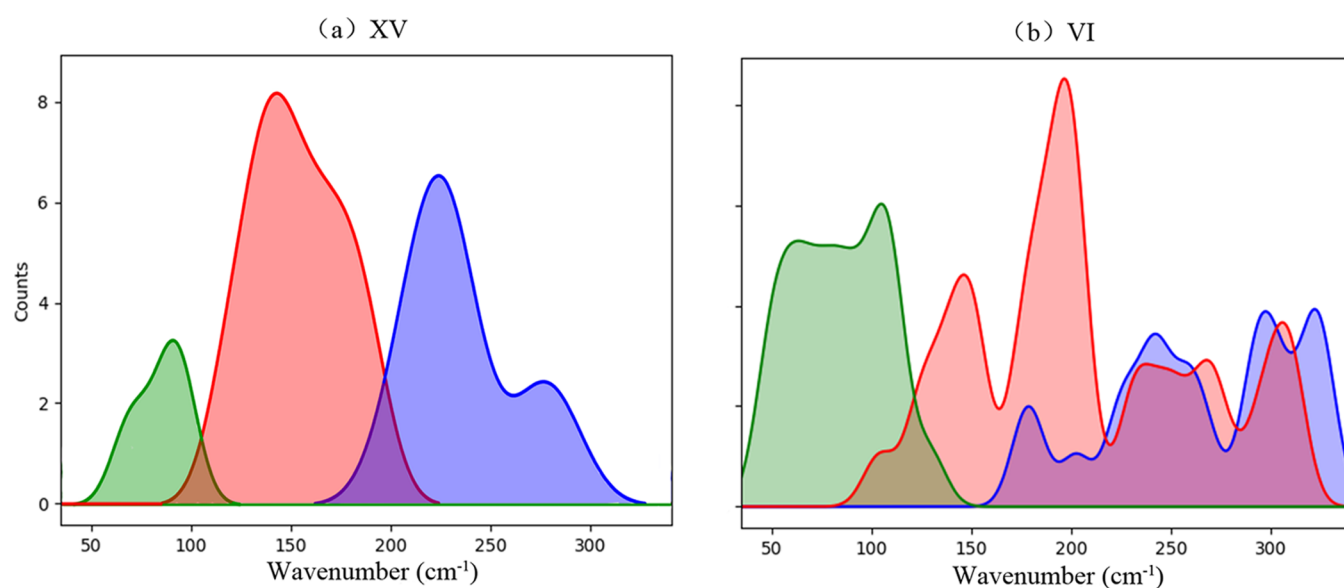


Figure 3. Comparison of fitted partial PDOS curves of (a) ice XV and (b) ice VI. Green represents non-H-bond modes, red represents two H-bond modes, and blue represents four H-bond modes.

185 cm^{-1} in the IR spectrum,⁴⁴ with a shoulder extending to 295 cm^{-1} . In the stretching band, the simulated peak at 423.13 meV (3405.82 cm^{-1}) corresponds to the 424 meV (3412.82 cm^{-1}) peak in the INS spectrum.^{45,46} As the revised Perdew–Burke–Ernzerhof (RPBE) functional underestimates intermolecular interactions, calculations from a setup at higher pressure show better agreement with the experimental data.

Subject to Bernal–Fowler rules,⁴⁷ every water molecule in an ice phase forms a hydrogen bond (H bond) with each of its four neighbors, thus forming a tetrahedral structure. In 1996, Li collected the INS spectra of several ice phases and identified two characteristic H-bonding peaks in the molecular translation band.⁴⁵ The typical two triangular peaks of ice Ih (ordinary ice) were present at 28 and 37.5 meV. Under high pressure, the local tetrahedral structure of ice VI is deformed, resulting in the two main peaks shown in Figure 1. In 2012, we introduced the first density functional theory (DFT) calculations for ice Ih.²⁹ Notably, based on the harmonic approximation, DFT calculations of the vibrational spectrum of ice Ih were in good agreement with experimental data. We also performed a series of computational investigations on the vibrational spectra of ice phases to determine the origin of the two H-bond peaks in the translation band. We have recently proposed that these two peaks represent two main groups of intrinsic molecular translational vibrations,⁴⁰ which have a strength ratio of approximately $\sqrt{2}$ in ideal hydrogen-ordered ice Ic.³² In the strong mode, a molecule vibrates along the H–O–H angle bisector against its four H-bonded neighbors, which is denoted as four-bond mode vibration. In the weak mode, a molecule vibrates in a direction perpendicular to the four-bond mode; this involves only the stretching of two H bonds, and is denoted as two-bond mode vibration. Herein, we focus on the H-bond vibrations of ice VI.

It is difficult to distinguish the atomic and molecular vibrations in an 80 molecule supercell from those of a simulated normal mode. In our previous work on ice XV, we found that there are three types of molecular translation vibrating modes. The lowest-energy vibrations represent relative movement between two sublattices. These two sublattices are interpenetrated but are not interconnected by

H bonds; thus, these non-H-bonding vibrations are of much lower strength. The two kinds of stronger H-bonding vibrational normal modes can be clearly seen in ice XV. We found that the molecular translation movement in ice VI approximately corresponds to the previously mentioned cluster (non-H-bond), two-bond, and four-bond vibrations. Figure 2a depicts a non-H-bond vibration in which the two sublattices exhibit motion in opposite directions. For the dynamic process, please see the video in the Supporting Information (SI). Figure 2b depicts a two-bond vibration mode in which many molecules vibrate with two H-bonded neighbors. Figure 2c depicts a four-bond vibration mode, in which it can be seen that with the left bottom molecule vibrates along its H–O–H angle bisector, as shown by the gold arrows. The four H bonds connected with neighbors vibrate together. In this case, the four-bond vibrational mode is stronger than the two-bond vibrational mode (see the dynamic processes of the above three vibrational modes in the Supporting Information, Figure 2). In addition, there is an “isolated stretching mode,” during which only one O–H vibrates in the stretching band of ice XV; this was first proposed to be a new mode by Whale et al.²⁷ We also observed this phenomenon in many kinds of ice phases and attributed it to pressure and a hydrogen-disordered lattice causing tetrahedral deformation.²⁸ Figure 2d depicts such a special stretching mode at 3378 cm^{-1} in ice VI (also see the Supporting Information, Figure 2). We regard this as an asymmetric stretching mode.

Figure 3 presents the partial PDOS of the non-H-bond, two-bond, and four-bond vibrational normal modes of ice XV and ice VI, respectively. We use a self-compiled program (see the SI file of ref 40) to categorize the two kinds of H-bond modes and obtain fitting images together with cluster modes, as shown in Figure 3. In this simulation, the average H-bond length of ice XV is 1.939 Å and that of ice VI is 1.870 Å. The shorter the H-bond length, the greater the H-bond strength, and thus the translation band of ice VI is blue-shifted than that of ice XV. It is difficult to clarify the vibrational modes of ice VI as so many molecules vibrate within one supercell. Considering that the mass center of a supercell remains static in an optical vibrational mode, all of the molecular vibrations in a supercell

should be coupled. Thus, we selected the molecule that had the largest amplitude vibration to represent the mode type. Based on the vibrating direction of oxygen in this molecule, a self-compiled program was used to classify mode type automatically, as we have recently reported.⁴⁰

Figure 3 presents a comparison between ice XV and ice VI, demonstrating that the three H-bond modes of ice XV are substantially separated, whereas the two kinds of H-bond modes of VI are overlapped. This latter result is due to local deformation of the tetrahedral H-bonding lattice originated from hydrogen disorder, which causes the boundary between two-bond modes and four-bond modes to be unclear. Correspondingly, there is a larger red shift in the stretching band of ice VI than in that of ice XV. We found that the most prominent Raman peak was at 3209 cm^{-1} , which corresponds to the peak at 3214 cm^{-1} calculated by Thoeny et al.⁴⁷ and that at 3204 cm^{-1} calculated by Marckmann et al.⁴⁸

3. CONCLUSIONS

We used first-principles DFT to simulate the vibrational spectrum of ice VI and compared this with that of its hydrogen-ordered counterpart, ice XV. We found similarities between these spectra, especially in the translation band. Inspired by the hydrogen-ordered structure of ice XV, we analyzed the normal modes of ice VI and found that it also obeys the two H-bond theory.

Due to the hydrogen-disordered structure of ice VI, the boundary between the two kinds of H-bond phonons in ice VI is not as clear as that in ice XV. Thus, two main H-bond peaks can be seen in this region in the INS spectrum. There are also many non-H-bond vibrations visible in the translational band at much lower energy, which represent vibrations between two sublattices. In the stretching band, we also found an “isolated stretching” mode, which was previously proposed by Whale et al. We regard this as a special asymmetric mode created by pressure and the hydrogen-disordered local structure.

We compared a small primitive cell and a large supercell to determine the differences in the vibrational spectra between ice XV and VI. This revealed that two H-bond vibration modes are applicable in ice VI.

4. COMPUTATIONAL METHODS

As ice VI is hydrogen-disordered, it does not have a periodic repeating unit. Thus, to mimic its structure, we constructed a $2 \times 2 \times 2$ ice XV supercell containing 80 molecules. We used a self-compiled program to generate hydrogens automatically. As the number of possible permutations of hydrogens is very large, we reduced this number by restricting the search to those permutations that had a uniformly distributed dipole moment. The permutation having the minimum polarizability was selected as the ice VI model (see the Supporting Information, Figure 1). The geometrical optimization and phonon calculations were conducted using the Cambridge Serial Total Energy Package (CASTEP),⁴⁹ a first-principles density functional theory (DFT) method. For the exchange–correlation (XC) functional, the generalized gradient approximation (GGA) RPBE⁵⁰ was selected for this work, based on ice XV calculations.²⁸ The energy and self-consistent field tolerances were set as 1×10^{-3} eV/atom for geometrical optimization with norm-conserving pseudopotentials. The energy cutoff was set at 750 eV and the γ -point for ice VI was used for k -point sampling. The original density of the

model was 1.40 g/cm^3 , and after we tested the hydrostatic pressure for geometrical optimization at 0, 0.9, and 2 GPa, the optimized densities were 1.10, 1.21, and 1.30 g/cm^3 , respectively. As the experimental density of ice VI is 1.33 g/cm^3 , we chose the 2 GPa density (1.30 g/cm^3) for the subsequent phonon calculations.

To determine the number of different H-bond vibrational modes, we compiled a customized program to distinguish the mode types.⁴⁰ As reported in our previous studies, the program classifies the main vibrational vector of oxygen as either a two-bond mode or a four-bond mode vibrational vector.

■ ASSOCIATED CONTENT

Supporting Information

The Supporting Information is available free of charge at <https://pubs.acs.org/doi/10.1021/acsomega.1c01315>.

Four typical H-bond vibration modes (MP4)

■ AUTHOR INFORMATION

Corresponding Author

Peng Zhang – School of Space Science and Physics, Shandong University, Weihai 264209, Shandong, China; orcid.org/0000-0002-1099-6310; Email: zhangpeng@sdu.edu.cn

Authors

Xue-Chun Wang – School of Space Science and Physics, Shandong University, Weihai 264209, Shandong, China; orcid.org/0000-0001-7839-3842

Xu-Liang Zhu – School of Space Science and Physics, Shandong University, Weihai 264209, Shandong, China

Yue Gu – School of Space Science and Physics, Shandong University, Weihai 264209, Shandong, China

Hao-Cheng Wang – School of Space Science and Physics, Shandong University, Weihai 264209, Shandong, China

Xiao-Ling Qin – School of Space Science and Physics, Shandong University, Weihai 264209, Shandong, China

Jing-Wen Cao – School of Space Science and Physics, Shandong University, Weihai 264209, Shandong, China; orcid.org/0000-0002-3226-3281

Xu-Hao Yu – School of Space Science and Physics, Shandong University, Weihai 264209, Shandong, China

Xiao-Qing Yuan – School of Space Science and Physics, Shandong University, Weihai 264209, Shandong, China

Complete contact information is available at: <https://pubs.acs.org/doi/10.1021/acsomega.1c01315>

Notes

The authors declare no competing financial interest.

■ ACKNOWLEDGMENTS

This work was financially supported by the National Natural Science Foundation of China (grant no. 11075094). The numerical calculations were performed on the supercomputing system at the Supercomputing Center, Shandong University, Weihai.

■ REFERENCES

- (1) Tammann, G. Ueber die Grenzen des festen Zustandes IV. *Ann. Phys.* **1900**, *307*, 1–31.
- (2) Bridgman, P. W. Water, in the Liquid and Five Solid Forms, under Pressure. *Proc. Am. Acad. Arts Sci.* **1912**, *47*, 441.

- (3) Bridgman, P. W. The Phase Diagram of Water to 45,000 kg/cm². *J. Chem. Phys.* **1937**, *5*, 964.
- (4) Bridgman, P. W. The Pressure-Volume-Temperature Relations of the Liquid, and the Phase Diagram of Heavy Water. *J. Chem. Phys.* **1935**, *3*, 597.
- (5) Millot, M.; Coppari, F.; Rygg, J. R.; Barrios, A. C.; Hamel, S.; Swift, D. C.; Eggert, J. H. Nanosecond X-ray diffraction of shock-compressed superionic water ice. *Nature* **2019**, *569*, 251–255.
- (6) Bertie, J. E.; Whalley, E.; Calvert, L. D. Transformations of ice II, ice III, and ice V at atmospheric pressure. *J. Chem. Phys.* **1963**, *38*, 840.
- (7) Bertie, J. E.; Whalley, E. Optical spectra of orientationally disordered crystals. 2. Infrared spectrum of ice Ih and ice Ic from 360 to 50 cm⁻¹. *J. Chem. Phys.* **1967**, *46*, 1271.
- (8) Whalley, E.; Heath, J. B. R.; Davidson, D. W. Ice 9—An antiferroelectric phase related to ice 3. *J. Chem. Phys.* **1968**, *48*, 2362.
- (9) Tajima, Y.; Matsuo, T.; Suga, H. Phase-transition in KOH-doped hexagonal ice. *Nature* **1982**, *299*, 810–812.
- (10) Kuhs, W. F.; Finney, J. L.; Vettier, C.; Bliss, D. V. Effect of high-pressure on the Raman-spectra of ice-VIII and evidence for ice-X. *J. Chem. Phys.* **1984**, *81*, 3612–3623.
- (11) Hirsch, K. R.; Holzapfel, W. B. *J. Chem. Phys.* **1986**, *84*, 2771.
- (12) Lobban, C.; Finney, J. L.; Kuhs, W. F. The structure of a new phase of ice. *Nature* **1998**, *391*, 268–270.
- (13) Salzmann, C. G.; Radaelli, P. G.; Hallbrucker, A.; Mayer, E.; Finney, J. L. The preparation and structures of hydrogen ordered phases of ice. *Science* **2006**, *311*, 1758–1761.
- (14) Salzmann, C. G.; Radaelli, P. G.; Mayer, E.; Finney, J. L. Ice XV: A New Thermodynamically Stable Phase of Ice. *Phys. Rev. Lett.* **2009**, *103*, No. 105701.
- (15) Falenty, A.; Hansen, T. C.; Kuhs, W. F. Formation and properties of ice XVI obtained by emptying a type sII clathrate hydrate. *Nature* **2014**, *516*, 231.
- (16) del Rosso, L.; Celli, M.; Ulivi, L. New porous water ice metastable at atmospheric pressure obtained by emptying a hydrogen-filled ice. *Nat. Commun.* **2016**, *7*, No. 13394.
- (17) Gasser, T. M.; Thoeny, A. V.; Fortes, A. D.; Loerting, T. Structural characterization of ice XIX as the second polymorph related to ice VI. *Nat. Commun.* **2021**, *12*, No. 1128.
- (18) Gasser, T. M.; Thoeny, A.; Plaga, L.; et al. Experimental evidence for a second hydrogen ordered phase of ice VI. *Chem. Sci.* **2018**, *9*, 4224–4234.
- (19) McFarlan, R. L. Apparatus for x-ray patterns of the high pressure modifications of ice. *Rev. Sci. Instrum.* **1936**, *7*, 82–85.
- (20) McFarlan, R. L. The structure of ice II. *J. Chem. Phys.* **1936**, *4*, 60–64.
- (21) Bertie, J. E.; Whalley, E.; Calvert, L. D. Transformations of Ice II, Ice III, and Ice V at Atmospheric Pressure. *J. Chem. Phys.* **1963**, *38*, 840.
- (22) Block, S.; Weir, C. W.; Piermari, G. High-Pressure Single-Crystal Studies of Ice VI. *Science* **1965**, *148*, 947.
- (23) Kamb, B. Structure of Ice VI. *Science* **1965**, *150*, 205.
- (24) Kuhs, W. F.; Finney, J. L.; Vettier, C.; Bliss, D. V. Structure and Hydrogen Ordering in Ices VI, VII, and VIII by Neutron Powder Diffraction. *J. Chem. Phys.* **1984**, *81*, 3612–3623.
- (25) Li, J. C.; Londono, J. D.; Ross, D. K.; Finney, J. L.; Tomkinson, J.; Sherman, W. F. An inelastic incoherent neutron scattering study of ice II, IX, V, and VI—in the range from 2 to 140 meV. W. F. Sherman. *J. Chem. Phys.* **1991**, *94*, 6770–6775.
- (26) Fan, X.; Bing, D.; Zhang, J.; Shen, Z.; Kuo, J.-L. Predicting the hydrogen bond ordered structures of ice Ih, II, III, VI and ice VII: DFT methods with localized based set. *Comput. Mater. Sci.* **2010**, *49*, S170–S175.
- (27) Whale, T. F.; Clark, S. J.; Finney, J. L.; Salzmann, C. G. DFT-assisted interpretation of the Raman spectra of hydrogen-ordered ice XV. *J. Raman Spectrosc.* **2013**, *44*, 290–298.
- (28) Qin, X. L.; Zhu, X. L.; Cao, J. W.; Jiang, L.; Gu, Y.; Wang, X. C.; Zhang, P. Computational Analysis of Exotic Molecular and Atomic Vibrations in Ice XV. *Molecules* **2019**, *24*, No. 3115.
- (29) Zhang, P.; Tian, L.; Zhang, Z. P.; Shao, G.; Li, J. C. Investigation of the hydrogen bonding in ice Ih by first-principles density function methods. *J. Chem. Phys.* **2012**, *137*, No. 044504.
- (30) Zhang, P.; Wang, Z.; Lu, Y.-B.; Ding, Z.-W. The normal modes of lattice vibrations of ice XI. *Sci. Rep.* **2016**, *6*, No. 29273.
- (31) Yao, S.-K.; Zhang, P.; Zhang, Y.; Lu, Y.-B.; Yang, T.-L.; Sun, B.-G.; Yuan, Z.-Y.; Luo, H.-W. Computing analysis of lattice vibrations of ice VIII. *RSC Adv.* **2017**, *7*, 31789–31794.
- (32) Yuan, Z.-Y.; Zhang, P.; Yao, S.-k.; Lu, Y.-B.; Yang, H.-Z.; Luo, H.-W.; Zhao, Z.-J. Computational assignments of lattice vibrations of ice Ic. *RSC Adv.* **2017**, *7*, 36801–36806.
- (33) Zhang, K.; Zhang, P.; Wang, Z.-R.; Zhu, X.-L.; Lu, Y.-B.; Guan, C.-B.; Li, Y. DFT Simulations of the Vibrational Spectrum and Hydrogen Bonds of Ice XIV. *Molecules* **2018**, *23*, No. 1781.
- (34) Wang, Z.-R.; Zhu, X.-L.; Jiang, L.; Zhang, K.; Luo, H.-W.; Gu, Y.; Zhang, P. Investigations of the Hydrogen Bonds and Vibrational Spectra of Clathrate Ice XVI. *Materials* **2019**, *12*, No. 246.
- (35) Zhu, X.-L.; Yuan, Z.-Y.; Jiang, L.; Zhang, K.; Wang, Z.-R.; Luo, H.-W.; Gu, Y.; Cao, J.-W.; Qin, X.-L.; Zhang, P. Computational analysis of vibrational spectrum and hydrogen bonds of ice XVII. *New J. Phys.* **2019**, *21*, No. 043054.
- (36) Gu, Y.; Zhu, X.-L.; Jiang, L.; Cao, J.-W.; Qin, X.-L.; Yao, S.-K.; Zhang, P. Comparative Analysis of Hydrogen Bond Vibrations in Ice VIII and VII. *J. Phys. Chem. C* **2019**, *123*, 14880–14883.
- (37) Cao, J.-W.; Chen, J.-Y.; Qin, X.-L.; Zhu, X.-L.; Jiang, L.; Gu, Y.; Yu, X.-H.; Zhang, P. DFT Investigations of the Vibrational Spectra and Translational Modes of Ice II. *Molecules* **2019**, *24*, No. 3135.
- (38) Wei, Z.-W.; Zhu, X.-L.; Cao, J.-W.; Qin, X.-L.; Jiang, L.; Gu, Y.; Wang, H.-C.; Zhang, P. Two basic vibrational modes of hydrogen bonds in ice XIII. *AIP Adv.* **2019**, *9*, No. 115118.
- (39) Zhao, Z.-J.; Qin, X.-L.; Cao, J.-W.; Zhu, X.-L.; Yang, Y.-C.; Wang, H.-C.; Zhang, P. Computing Investigations of Molecular and Atomic Vibrations of Ice IX. *ACS Omega* **2019**, *4*, 18936–18941.
- (40) Zhu, X.-L.; Cao, J.-W.; Qin, X.-L.; Jiang, L.; Gu, Y.; Wang, H.-C.; Liu, Y.; Kolesnikov, A. I.; Zhang, P. Origin of Two Distinct Peaks of Ice in the THz Region and Its Application for Natural Gas Hydrate Dissociation. *J. Phys. Chem. C* **2020**, *124*, 1165–1170.
- (41) Abe, K.; Shigenari, T. Raman spectra of proton ordered phase XI of ICE I. Translational vibrations below 350 cm⁻¹. *J. Chem. Phys.* **2011**, *134*, No. 104506.
- (42) Li, J. C. Inelastic neutron scattering studies of hydrogen bonding in ices. *J. Chem. Phys.* **1996**, *105*, 6733–6755.
- (43) Rosu-Finsen, A.; Amon, A.; Armstrong, J.; Fernandez-Alonso, F.; Salzmann, C. G. Deep-Glassy Ice VI Revealed with a Combination of Neutron Spectroscopy and Diffraction. *J. Phys. Chem. Lett.* **2020**, *11*, 1106–1111.
- (44) Bertie, J. E.; Labbe, H. J.; Whalley, E. Infrared Spectrum of Ice VI in the Range 4000–50 cm⁻¹. *J. Chem. Phys.* **1968**, *49*, 2141.
- (45) Li, J. C.; Londono, D.; Ross, D. K.; Finney, J. L.; Bennington, S. M.; Taylor, A. D. Inelastic incoherent neutron scattering study of ice Ih, II, IX, V and VI in the region from 50–500 meV. *J. Phys.: Condens. Matter* **1992**, *4*, 2109–2116.
- (46) Bernal, J. D.; Fowler, R. H. A theory of water and ionic solution, with particular reference to hydrogen and hydroxyl ions. *J. Chem. Phys.* **1933**, *1*, 515–548.
- (47) Thoeny, A. V.; Gasser, T. M.; Loerting, T. Distinguishing ice beta-XV from deep glassy ice VI: Raman spectroscopy. *Phys. Chem. Chem. Phys.* **2019**, *21*, 15452–15462.
- (48) Marckmann, J. P.; Whalley, E. Vibrational Spectra of the Ices. Raman Spectra of Ice VI and Ice VII. *J. Chem. Phys.* **1964**, *41*, 1450–1453.
- (49) Clark, S. J.; Segall, M. D.; Pickard, C. J.; Hasnip, P. J.; Probert, M. I.; Refson, J. K.; Payne, M. C. First principles methods using CASTEP. *Z. Kristallogr.* **2005**, *220*, 567.
- (50) Hammer, B.; Hansen, L. B.; Norskov, J. K. Improved adsorption energetics within density-functional theory using revised Perdew-Burke-Ernzerhof functionals. *Physical Review B* **1999**, *59*, 7413–7421.